Spectrochimica Acta Part A: Molecular and Biomolecular Spectroscopy 309 (2024) 123867

Contents lists available at ScienceDirect

Spectrochimica Acta Part A:
Molecular and Biomolecular Spectroscopy

journal homepage: www.journals.elsevier.com/spectrochimica-acta-part-a-molecular-and-biomolecular-spectroscopy

# *In situ* Raman spectral observation of succinimide intermediates in amyloid fibrillation kinetics

Ning Chen [a,1], Yi Ren [b,1], Lei Xing [c,*], Zhongqiang Liu [b,*], Lin Chen [d], Shilin Liu [a], Xiaoguo Zhou [a,*]

[a] Department of Chemical Physics, University of Science and Technology of China, Hefei, Anhui 230026, China
[b] Key Laboratory of Tropical Biological Resources of the Ministry of Education, Department of Pharmaceutical Sciences, Hainan University, Haikou, Hainan 570228, China
[c] State Key Laboratory of Analytical Chemistry for Life Science, School of Chemistry and Chemical Engineering, Nanjing University, Nanjing 210023, China
[d] School of Physics and Materials Engineering, Hefei Normal University, Hefei, Anhui 230601, China

## HIGHLIGHTS

- A Raman spectral fingerprint to trace the succinimide intermediates in amyloid fibril formation is proposed.
- Succinimide intermediates are formed in denaturation process of lysozyme with thermal/acid treatment.
- Succinimide intermediates play an important role in the oligomer formation of lysozyme.

## GRAPHICAL ABSTRACT

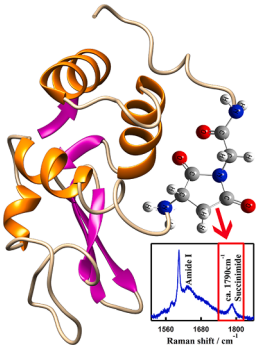


## ARTICLE INFO

*Keywords:*
Raman spectroscopy
Amyloid fibrils
Kinetics
Lysozyme
Succinimide

## ABSTRACT

Succinimide intermediates play the crucial role in the nucleation process for protein amyloid fibril formation, as they can usually induce a non-native conformation in a fraction of soluble proteins to render amyloidogenicity and neurotoxicity. Thus, *in situ* detection of succinimide intermediates during amyloid fibrillation kinetics is of considerable importance, albeit challenging, because these succinimides are generally unstable in physiological conditions. Here, we found an *in situ* Raman spectral fingerprint to trace the succinimide intermediates in amyloid fibril formation, wherein the carbonyl symmetric stretching of cyclic imide in the succinimide derivative is located at ca. 1790 $cm^{-1}$. Using its intensity as an indicator of succinimide intermediates, we have *in situ* detected and unravelled the role of succinimide intermediates during the oligomer formation from the Bz-Asp-Gly-$NH_2$ dipeptide or the amyloid fibrillation kinetics of lysozyme with thermal/acid treatment.

* Corresponding authors.
*E-mail addresses:* xl1992@nju.edu.cn (L. Xing), liuzhongqiang@gmail.com (Z. Liu), xzhou@ustc.edu.cn (X. Zhou).
[1] These authors contributed equally to this work.

https://doi.org/10.1016/j.saa.2024.123867
Received 22 September 2023; Received in revised form 28 December 2023; Accepted 5 January 2024
Available online 6 January 2024

## 1. Introduction

Neurodegenerative diseases like Parkinson's and Alzheimer's diseases, which affect approximately 30 million people worldwide, are characterized by deposits of amyloid-beta (Aβ) fibrils in certain regions of the brain.[1–3] In the amyloid fibril formation, conformational changes of native proteins, especially such as the formation of β-sheet-rich fibrillar aggregates, are often associated with protein degradation, degeneration, and cell toxicity.[1–3] For those proteins containing the Asp-Gly dipeptide structure, the formation of intermediates with succinimide motif has been thought to be one of the most significant elementary processes for the transformation of Aβ peptides, as shown in Scheme 1.[4–6] In physiological conditions, the side chain –COOH of the L-Asp residue can interact with an adjacent amide nitrogen on the peptidyl backbone to produce a five-member succinimide ring by eliminating one water molecule. In alkaline solutions, the intermediate with succinimide ring can be reopened to generate either D/L- aspartic or D/L- *iso*-aspartic acid, according to racemization and isomerization reactions.[5–7]

Although the above mechanism is widely accepted in the amyloid fibrillation kinetics of proteins,[8] directly identifying the intermediates with succinimide motif during amyloid fibril growth in experiments remains challenging. In 1993, Pistorius *et al.* performed a combined study of Fourier-transform infrared (FT-IR) and Raman spectroscopy on two peptides, H-Asp-Ala-OH and H-Val-Asp-Ala-Gly-OH, in the solid state.[9] For the succinimide which was derived from H-Asp-Ala-OH, the doublet centered around 1715 $cm^{-1}$ was attributed to the Fermi resonance of the antisymmetric imide carbonyl stretching, while the symmetric imide carbonyl stretching was located at 1793 $cm^{-1}$. To one's surprise, in the succinimide derivatives of the larger peptide, the Fermi resonance did not occur. This pioneering work provided a candidate for the spectral fingerprint for succinimide intermediates.[9] Moreover, the high-performance liquid chromatography-mass spectrometry (HPLC-MS) studies on the solid-state lysozyme[10,11] and lactoglobulin[12] were carried out, where fragment ions arising from $NH_3$ (–17 Da) or $H_2O$ (–18 Da) losses were detected, providing indirect evidence for the succinimide-ring formation. However, these studies of solid-state proteins cannot fully reveal the actual intra- and extracellular transformation processes, since amyloid formation in living organisms usually occurs in aqueous environment. Recently, succinimide derivatives formed in the amyloid growth of aqueous proteins with thermal/acid treatment have been indirectly verified by detecting the mass loss of $NH_3$– or $H_2O$–, using hydrogen/deuterium exchange or ion-exchange mass spectrometry.[7,14–17] Although these conclusions all point to the presence of the succinimide intermediates during amyloid fibril formation, *in situ* spectral observation of succinimide intermediates during amyloid fibril growth in aqueous solution remains elusive.

Hen egg white-lysozyme (HEWL) has been widely used as a model protein for studying amyloid fibril formation, because conformational changes of its peptidyl sequence from 57 to 107 are very similar to those of Aβ proteins associated with Alzheimer's diseases.[17–20] It is well known that HEWL can aggregate to form β-sheet-rich fibrils in various denaturing conditions, such as thermal and acidic treatment,[20] addition of metal ions,[21–31] small organic chemicals (folic acid[31], entacapone[32]), and nanoparticles[33]. A four-stage step-by-step transformation mechanism was proposed to describe kinetics of lysozyme amyloid fibrillation as a sequence of partial unfolding of the tertiary structures, α-helix breaking to form statistical coils and oligomers, formation of organized β-sheet structures, and supramolecular association of the β-sheets protofibrils to mature fibrils.[20] Notably, by adding extra succinimide into the lysozyme solution, it was found that the native disulfide bonds of lysozyme were broken more efficiently and quickly within hydrolysis, resulting in exposure of the buried hydrophobic residues and accelerating the formation of cross β-sheet structures by skipping intermediate random coils.[34] However, the role of succinimide-like intermediates formed from the Asp-Gly peptidyl structure in protein denaturation process in acidic solutions is unclear to date.

To simulate this natural process, a dipeptide derivative, Bz-Asp-Gly-$NH_2$, was herein synthesized with the N- and C-termini capped, respectively, by a benzoate (Bz) to improve peptide hydrophobicity and an –$NH_2$ group to mimic the next amide bond in long peptides or proteins. Using the core, we applied spontaneous Raman spectroscopy in combination with mass spectrometry and thioflavin (ThT) fluorescence to observe, *in situ*, the succinimide intermediates during amyloid fibril growth in the dipeptide and HEWL solutions. A spectral fingerprint of the succinimide motif was identified in both dipeptide and lysozyme solutions.

## 2. Experimental and computational

### 2.1. Synthesis and characterization of Bz-Asp-Gly-$NH_2$ dipeptide

As the π interaction between side chains can stabilize the succinimide motif,[14,15] the n + 1 residue Gly was suggested to protect succinimide derivatives from hydrolysis in extreme conditions.[13,36–38] Thus, Bz-Asp-Gly-$NH_2$ was selected as the model dipeptide for studying the formation and influence of succinimide derivatives. The synthesis was performed using a standard protocol of Fmoc-based solid-phase peptide synthesis in Scheme S1.

### 2.2. Solution preparation

The Bz-Asp-Gly-$NH_2$ dipeptide was dissolved in a mixed solvent of acetonitrile and water (1:4 vol ratio) at room temperature. HEWL was purchased from Sangon Biotech (Shanghai) Co. Ltd. and was used without further purification. The thermal and acidic treatment was applied for the amyloid fibril formation of dipeptide and/or lysozyme, as previously described.[38–41] Briefly, the pH 2.0 solutions (10 mg/mL for the dipeptide or 20 mg/mL for the lysozyme) in sealed glass vials were incubated in a thermoshaker incubator at 65 °C without agitation. Aliquots of fibril-forming solution were taken out of the incubation vial at some specific times. The gelatinous phase formed during incubation was separated by centrifugation at 12,000*g* for 20 min. The residual supernatant (soluble fraction) was directly used in spontaneous Raman spectroscopy, ThT fluorescence assay, and atomic force microscopy (AFM) experiments.

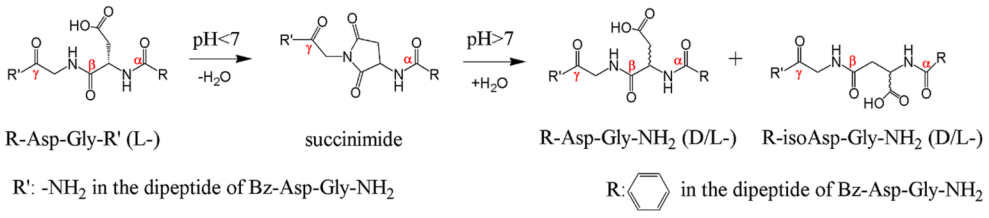


**Scheme 1.** Formation of the succinimide motif from an aspartyl peptide of R-Asp-Gly-R′ (L–).

### 2.3. Spontaneous Raman spectroscopy

The Raman spectrometer has been described previously,[41–45] and only a brief introduction is given here. The sample solution was kept in a 10 mm × 10 mm quartz cuvette at 25 °C without stirring. A CW laser (Coherent, Verdi V5, 532 nm) was employed as excitation light with the power of 4 W. The polarization of the laser was controlled by a half-wave plate. The parallel and perpendicular polarization components of Raman scattering light were selected using a Glan-Taylor polarizer. The scattering light was dispersed by a triple monochromator system (Acton Research, TriplePro) and recorded by a liquid-nitrogen-cooled CCD detector (Princeton Instruments, Spec-10:100B, controlled by an ST-133 controller). The Raman shift was carefully calibrated using the standard spectral lines of a mercury lamp. The spontaneous Raman spectra were recorded in the region of 300–1850 $cm^{-1}$ with the resolution of ca. 1 $cm^{-1}$. In experiments, the acquisition time for each measurement was 1 min, and 10 acquisitions were averaged for achieving better signal-to-noise ratios. In addition, to subtract background of the solvent, additional Raman spectra of HCl/water (*p*H 2.0) were recorded in identical conditions.

### 2.4. ThT fluorescence assays

At each specific incubation time, 40 μL aliquots of the supernatant were taken from vials, and were added to 960 μL ThT solutions (the concentration of ThT solution was ~1 × $10^5$ mol/L). The steady-state fluorescence emission spectra were measured with photoexcitation at 408 nm using a homemade fluorescence spectrometer, within a wavelength range of 400–800 nm, where a fiber optic spectrometer (AvaSpec-ULS2048, Avantes) was used to collect and detect the scattering light at 90 degrees. The excitation laser power was as low as 20 mW to ensure no saturation effect. Fluorescence assays were performed *ex situ* for the solutions immediately in ambient conditions.

### 2.5. AFM imaging

At each specific time, the supernatant was diluted 100 times with Milli-Q water, and then dropped onto freshly cleaved mica. Fifteen minutes later, the protein solution was rinsed off three times with deionized water. The mica surface was naturally dried at room temperature and was stored in a desiccator. All AFM imaging were performed on these air-dried samples with a Veeco DI-MultiMode V scanning probe microscope in tapping mode using the 5 μm × 5 μm or 2 μm × 2 μm scanners. The AFM height images were reconstructed using the NanoScope v9.2 software.

### 2.6. Quantum chemical computations

All density functional theory (DFT) calculations were performed using the Gaussian-09 program package.[45] The geometries of the dipeptide Bz-Asp-Gly-$NH_2$, succinimide, isoaspartic acid, and amino acids (Asp and Gly) were optimized at the B3LYP/PVTZ level of theory. Using the optimized geometries, harmonic vibrational frequencies and Raman intensities were calculated at the same level. Then, Raman spectra were simulated with the scaled vibrational frequencies by the factor of 0.98 [46] and the corrected intensities using the Gaussian output as described in the reference [47].

## 3. Results and discussion

### 3.1. Identification of succinimide intermediates by mass spectrometry

As mentioned above, the succinimide ring formation was affirmed by mass spectrometry previously in acidic dehydration processes of the solid-state peptides, H-Asp-Ala-OH and H-Val-Asp-Ala-Gly-OH[9], and lysozyme[10,11]. Likewise, electrospray ionization (ESI) MS and collision-induced dissociation (CID)-MS/MS analyses were conducted here for the aggregation products of the dipeptide Bz-Asp-Gly-$NH_2$ after thermal/acid treatment for 96 h, to identify the formation of succinimide intermediates along with the route in Scheme 1.

The native dipeptide was identified in mass spectra according to the appearance of the $[Bz\text{-}Asp\text{-}Gly\text{-}NH\text{-}Na]^+$ ion peak of *m/z* 316.09061 Da (Fig. 1a). After incubation in acidic conditions, a fragment ion (*m/z* 276.09839 Da) arising from the $H_2O$ (–18 Da) molecule loss was dominantly detected in the ESI-MS spectrum of the oligomers (Fig. 1b), implying the formation of succinimide-like intermediates. In contrast, this fragment ion was not observed in alkaline oligomer solutions (Fig. 1c). $^{13}C$ nuclear magnetic resonance (NMR) analysis was performed on the Bz-Asp-Gly-$NH_2$ peptide and the oligomers in acidic and alkaline solutions (Figure S2). Notably, no peak was observed in the $^{13}C$ NMR spectrum of the oligomer in alkaline solution within the range of 45–53 ppm, whereas the native-state Bz-Asp-Gly-$NH_2$ contributed a strong peak at $\delta$ 50.85, corresponding to the chiral, tertiary carbon of Asp. This implies that either the initial Bz-Asp-Gly-$NH_2$ had been consumed or its remaining trace amount was beyond detection by $^{13}C$ NMR. All these evidences are consistent with the formation mechanism of succinimide intermediates as indicated in Scheme 1.

### 3.2. Raman spectra of dipeptide and oligomers as aggregation products

Raman spectra of dipeptides in the native state and oligomers, which were formed in acidic and alkaline solutions after incubation for 96 h, were recorded in the range of 1500 to 1850 $cm^{-1}$ (Fig. 2), where a few sensitive vibrational bands were included, such as C = O symmetric stretching, ring stretching of benzene, and amide I band. Notably, the amide I band is composed of C = O stretching, C–N stretching, and N–H in-plane bending modes,[48] and covers the whole frequency range as a broad peak, while the other vibrational bands are superimposed over it as a few sharp and weak peaks, as shown in Fig. 2. In this scenario, second derivative spectra (in red) are used to identify the resonance frequencies of the vibrational bands. For comparison, the simulated Raman spectra at the B3LYP/CC-PVQZ level are also plotted there. Moreover, the depolarization ratios, $\rho$, of these vibrational peaks were experimentally determined as $\rho = I_V/I_P$, where $I_V$ and $I_P$ are the measured intensities of the perpendicular and parallel polarization Raman scattering, respectively.

Frequencies, intensities and depolarization ratios of the calculated and experimental vibrational bands are all summarized in Table 1. For an asymmetric vibrational band, $\rho$ usually equals 0.75, but it is much less for the symmetric modes. Thus, comparing the experimental and simulated spectral results, the observed vibrational peaks were all unambiguously assigned. For example, for the native-state dipeptide (Fig. 2a), the sharp, strong peak at 1604 $cm^{-1}$ was attributed to the phenyl moiety ring stretching,[49] and the weak peak at 1581 $cm^{-1}$ (noted with asterisks) was assigned to the C-terminus amide stretching vibration and the Fermi resonance band of phenyl ring stretching. Among three calculated peaks at 1637, 1656, and 1682 $cm^{-1}$ contributed by three dipeptide amide groups, only the strongest one at 1637 $cm^{-1}$ was presented in the experimental spectrum but it was significantly broadened due to complex conformations in aqueous solutions. In addition, although our calculation suggested that the –COOH carbonyl stretching vibration was located at 1749 $cm^{-1}$ (noted with green arrows), it was invisible in the experiments due to its relatively low scattering intensity (Table 1). On the other hand, hydrogen bonding also might cause this peak to obscure by red-shift to the broad amide I band. [50].

After incubation for 96 h in acidic conditions, spheroidal oligomers were predominantly formed, as shown in the AFM images (Fig. 4 in Section 3.3). A new peak at 1786 $cm^{-1}$ (noted with a cross in Fig. 2b) was clearly observed in the Raman spectra of oligomers, in comparison to that of the native-state dipeptide. Its peak position (1786 $cm^{-1}$) and enhanced intensity greatly agreed with the calculated harmonic

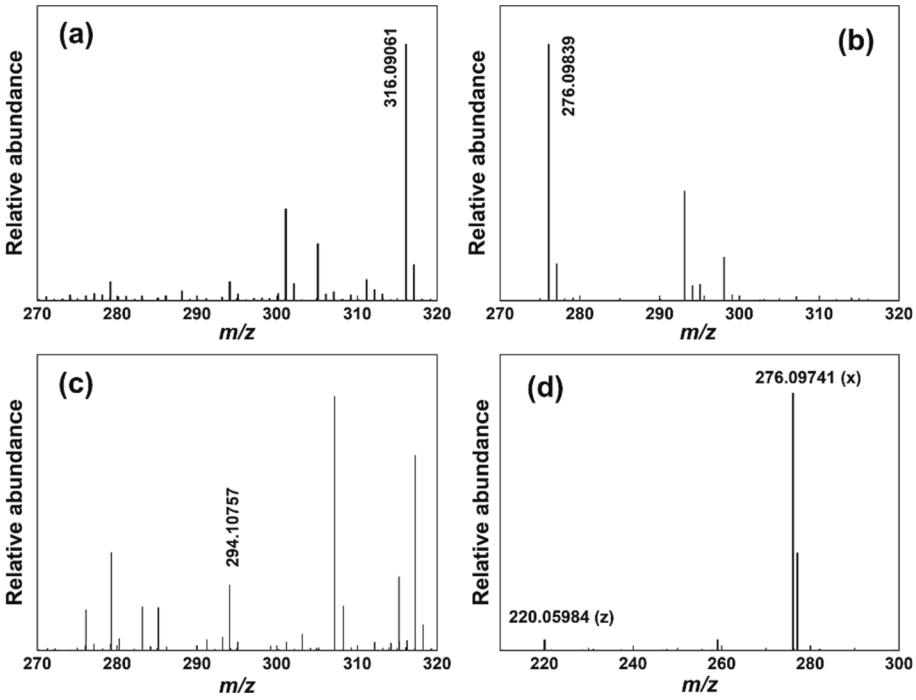


**Fig. 1.** ESI-MS images of the native-state dipeptide Bz-Asp-Gly-$NH_2$ (a), the oligomers formed in acidic solution (b) and the alkaline solution (c), where the 316.09061 Da is the mass of $[Bz\text{-}Asp\text{-}Gly\text{-}NH\text{-}Na]^+$. (d) CID-MS/MS spectra of the oligomers in alkaline solution, where the peptides (220.05984 and 276.09741 Da) were subjected to fragmentation of the dipeptide in (c). The x and z in (d) refer to the fragment ions shown in Scheme S2.

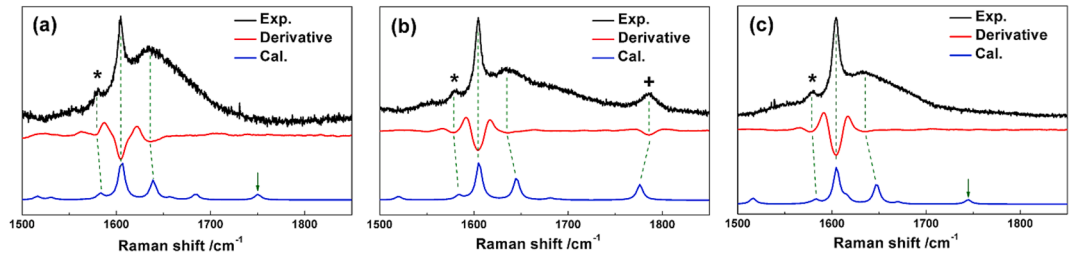


**Fig. 2.** Experimental (black line), and 2nd derivative (red line) Raman spectra of the native dipeptide (a), as well as the oligomers in acidic (b) and alkaline (c) solutions. The calculated Raman spectra of the dipeptide (a), succinimide derivative (b), and isoaspartic acid (c) are plotted with blue lines to compare with the experimental data.

frequency (1776 $cm^{-1}$) and the significantly increased Raman scattering intensity of the carbonyl symmetric stretching of the succinimide ring. The $\rho$ value of this peak was experimentally determined to be 0.21, which also was consistent with the calculated value (0.24). In contrast, neither experimental measurements nor theoretical calculations show visible change in the peak positions of the ring stretching of benzene and amide I bands during the dipeptide aggregation process. Moreover, along with the formation of spheroidal oligomers, a significant broadening of the amide I band width occurred, in line with the fact that disordered structures were dominant in micro-structure of oligomers. [51] In addition, the Raman spectrum of the oligomer formed in alkaline solutions was very similar to that of the dipeptide in native state, as shown in Fig. 2c, where the peak at 1786 $cm^{-1}$ disappeared. This phenomenon provides solid evidences for the formation of the five-member succinimide ring in acidic solutions and the racemization and isomerization in alkaline solutions, as illustrated in Scheme 1.

Additionally, to further verify the spectral assignment of succinimide intermediates, we need to exclude the contributions of the amino acids, Asp or Gly, or their combination from the peak at 1786 $cm^{-1}$. Thus, Raman spectra of the solution of Asp and Gly monomers (1:1 mass ratio) were measured and shown in Fig. 3. As the intramolecular –OH bending mode in $HCl/H_2O$ solution ($p$H 2.0) contributed a wide peak with the center at ~ 1640 $cm^{-1}$,[53,53] the contributions of Asp and Gly monomers could be easily identified in the difference spectrum (red trace in Fig. 3) by directly subtracting the solvent background.

For the Asp and Gly monomers, the calculated peak positions of –COOH carbonyl stretching vibration are located at 1721 and 1737 $cm^{-1}$ (with green arrow), and those of the amino stretching vibration are at 1570 and 1588 $cm^{-1}$ (noted with asterisks), respectively. These calculated peaks generally agree with the experimental spectrum, as shown in Fig. 3. Notably, no peaks were observed in experiments within the 1760 to 1850 $cm^{-1}$ range, where the spectral trace of succinimide intermediate is proposed. This indirectly validates our spectral assignment of the vibrational peak at 1786 $cm^{-1}$, that is attributed to the succinimide motif formed in the aggregation process of the dipeptide in acidic solutions.

Together, during incubation at pH 2.0 and 65 °C, Bz-Asp-Gly-$NH_2$ physically aggregates to form oligomers while chemically undergoing intramolecular cyclization to generate the succinimide-like motif. The symmetrical carbonyl stretching thereof contributes a new Raman vibrational band at 1786 $cm^{-1}$, serving as a novel spectral fingerprint for the succinimide-like intermediates.

**Table 1**
Calculated and experimental vibrational frequencies, Raman scattering intensities and depolarization ratios ($\rho$) of the dipeptide Bz-Asp-Gly-$NH_2$, the succinimide derivative and isoaspartic acid in the frequency range of 1500–1850 $cm^{-1}$.

| $\nu$ /$cm^{-1}$ | | Intensity[b] | $\rho$ [a,b] | Assignment |
|---|---|---|---|---|
| Cal.[a] | Exp. | | | |
| *Dipeptide* | | | | |
| 1749 | | 43 | (0.22) | C = O stretching of –COOH |
| 1682 | | 43 | (0.07) | Amide I (β–) |
| 1656 | | 14 | (0.57) | Amide I (γ–) |
| 1637 | 1636 | 141 | 0.22 (0.21) | Amide I (α–) |
| 1604 | 1605 | 286 | 0.53 (0.52) | Ring stretching of benzene |
| 1581 | 1580 | 41 | 0.31 (0.33) | Ring stretching of benzene |
| *Succinimide* | | | | |
| 1776 | 1786 | 118 | 0.21 (0.24) | C = O symmetric stretching of cyclic imide |
| 1691 | | 4 | (0.68) | C = O asymmetric stretching of cyclic imide |
| 1680 | | 15 | (0.56) | Amide I (γ–) |
| 1643 | 1636 | 161 | 0.21 (0.19) | Amide I (α–) |
| 1604 | 1604 | 273 | 0.53 (0.52) | Ring stretching of benzene |
| 1582 | 1579 | 31 | 0.26 (0.32) | Ring stretching of benzene |
| *isoaspartic acid* | | | | |
| 1744 | | 33 | (0.40) | C = O stretching of –COOH |
| 1669 | | 13 | (0.48) | Amide I (γ–) |
| 1646 | 1636 | 146 | 0.22 (0.20) | Amide I (α–) |
| 1614 | | 39 | (0.27) | Amide I (β–) |
| 1603 | 1605 | 262 | 0.54 (0.52) | Ring stretching of benzene |
| 1581 | 1579 | 27 | 0.35 (0.39) | Ring stretching of benzene |

[a] Scaled with a factor of 0.98.
[b] The values in parentheses are the calculated data.

### 3.3. AFM images for the aggregation process of dipeptide and HEWL

AFM images can directly show morphological changes of dipeptide and protein during their aggregation processes, providing clues for us to understand the relationship between morphology and structures of molecular assemblies. Fig. 4 shows the AFM images of the aggregate morphologies of the Bz-Asp-Gly-$NH_2$ dipeptide and HEWL at specific incubation times with thermal/acid treatment. Both the dipeptide and protein exhibit similar change trends in morphology during the initial incubation period. At the very early stage, the formed "seeds" of aggregates are too small to be observed. Several hours later, some aggregates of both dipeptide and protein begin to appear and gradually grow into spheroidal oligomers (Fig. 4b, 4c and 4d). However, no fibril-like assemblies were formed for the Bz-Asp-Gly-$NH_2$ aggregation, even after incubation for 96 h. This is understandable because protofibrils, the mandatory intermediates of amyloid fibril-like formation,[51] cannot be produced from the dipeptides due to the absence of protein strands.

For the HEWL solution, once spheroidal oligomers are formed, they can assemble into protofibrils (average height 8 nm after 96 h as shown in Fig. 4e), and then mature lysozyme fibrils are gradually formed from the further assembly of the protofibrils (Fig. 4f). Finally, the mature fibrils have approximately a few microns in length and are much stiffer than the protofibrils. Actually, the current morphological changes in the denaturation kinetics of HEWL in thermal and acidic solutions are in exact agreement with the previous studies.[40,55–57] Therefore, considering the similarities and differences in the denaturation processes of the dipeptide and protein, we can infer that the succinimide intermediates might only play a significant role in the oligomer formation throughout the whole kinetics of amyloid fibrillation formation.

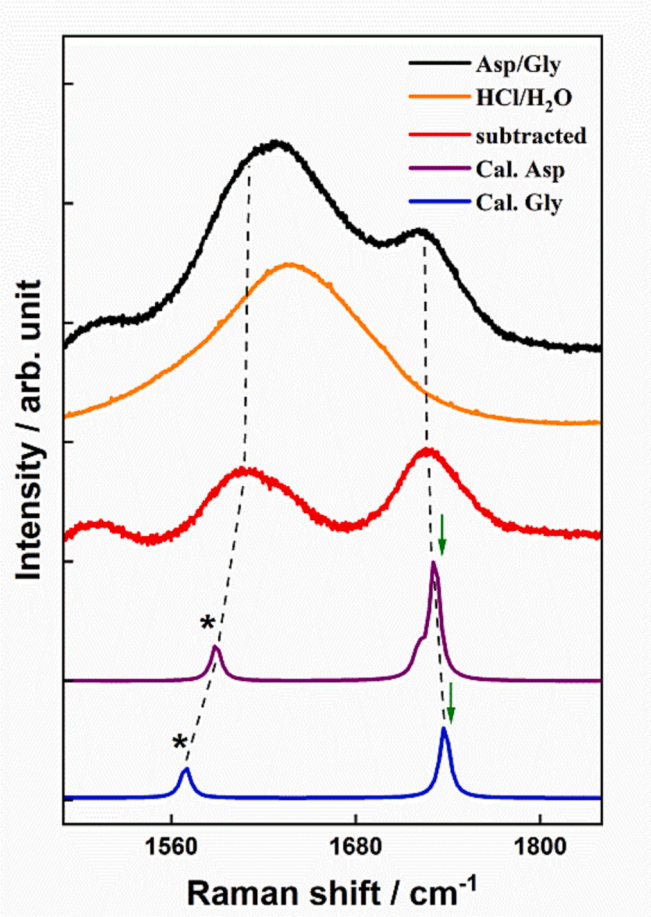


**Fig. 3.** Experimental Raman spectra of the Asp/Gly (1:1 mass ratio) solution (in black) and the $HCl/H_2O$ (*p*H 2.0) solution (in brown) with thermal/acid treatment, as well as their difference spectrum (in red). The calculated Raman spectra of the Asp (in purple) and Gly (in blue) monomers are plotted too.

### 3.4. Raman spectra in the overall amyloid fibrillation kinetics of HEWL

Using the Raman indicator at 1786 $cm^{-1}$ for the succinimide intermediates, Raman spectroscopy was applied to unravel their roles *in situ* during amyloid fibril formation of HEWL with thermal/acid treatment. Actually, the overall amyloid fibrillation kinetics of HEWL in thermal and acidic solutions have been studied previously using Raman spectroscopy.[20] with two indicators for secondary structures (the N-$C_\alpha$-C stretching vibration at 933 $cm^{-1}$ and the amide I band in the range of 1640–1680 $cm^{-1}$) and the Raman marker for tertiary structures as the full width at half maximum (FWHM) of the Trp residues at 758 $cm^{-1}$.

Fig. 5 shows the comparison of the Raman spectra of the HEWL in native state and the mature fibrils in the regions of 700–1030 and 1570–1830 $cm^{-1}$. Similar to the previous conclusions,[20] the peak intensity at 933 $cm^{-1}$ contributed by the N-$C_\alpha$-C stretching vibration of α-helixes[40] was markedly reduced for the fibrils, indicating a loss of α-helix structure during amyloid formation. For another indicator of protein secondary structures, the amide I peak position, a visible blue-shift of 12-$cm^{-1}$ was observed from the native state to the fibrils. Considering that the band mainly consists of C = O and C–N stretching, with a small amount of N–H in-plane bending vibration,[48] different secondary structures have specific peak positions, for instance, α-helical structure covers 1650–1660 $cm^{-1}$,[40] β-sheets are mainly located at 1671–1673 $cm^{-1}$,[20,57] β-turns and random structures are in

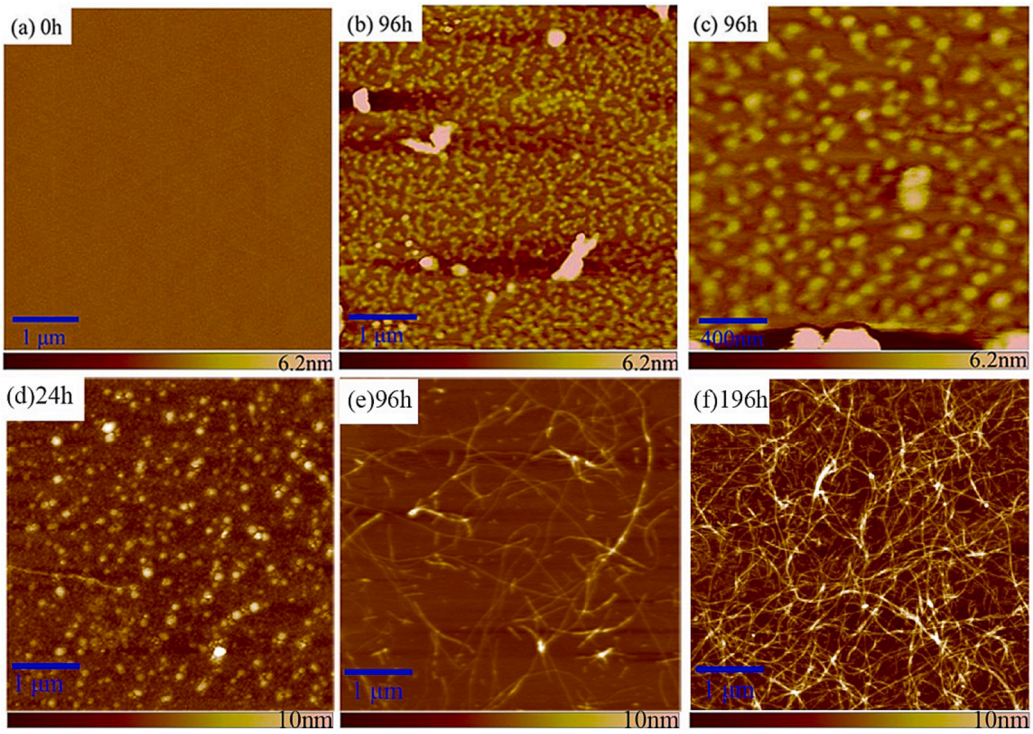


**Fig. 4.** AFM images of the dipeptide of Bz-Asp-Gly-$NH_2$ and HEWL with thermal/acid treatment (65 °C, *p*H 2), (a-c) for the dipeotide at 0 and 96 h, and (d-f) for the HEWL at 24, 96, and 196 h, respectively.

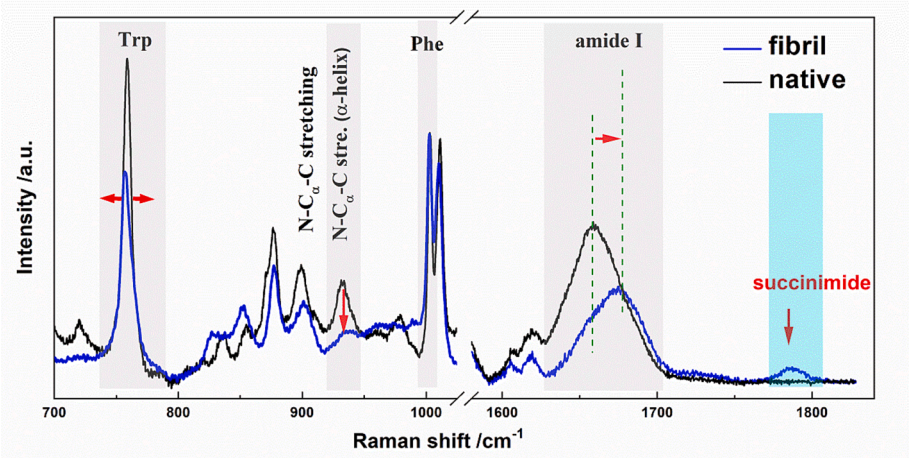


**Fig. 5.** Raman spectra of HEWL in the native state (in black) and fibrils (in blue), in the ranges of 860–970, 1210–1380 and 1570–1880 $cm^{-1}$, where the intensities are normalized with the Phe peak intensity at 1003 $cm^{-1}$.

1670–1680 $cm^{-1}$,[58] extended PP II in protofibril is at 1667 $cm^{-1}$,[59] and β-intermolecular and intramolecular structures are located at 1669 and 1682 $cm^{-1}$,[60] respectively. Hence, the observed blue-shift of the amide I peak undoubtedly confirms the transformation from α-helix to β-sheets.

Notably, a distinct peak at 1790 $cm^{-1}$ was clearly observed in the Raman spectrum of mature lysozyme fibrils, in comparison to that of the native HEWL. As discussed above, this peak is the sensitive indicator for the succinimide-like intermediates, and thus its appearance in the fibril spectra implies that the succinimide intermediates are visibly produced in the amyloid fibrillation kinetics of HEWL in thermal and acidic conditions. Therefore, by *in situ* monitoring and comparing this indicator and other spectral markers of the secondary and tertiary structures of protein such as the FWHM of the Trp residue band at 758 $cm^{-1}$, the amide I peak position, and the intensity at 933 $cm^{-1}$, the role of succinimide intermediates can be uncovered in the various stages of the overall HEWL amyloid formation process.

### 3.5. Comparison of the amyloid fibrillation kinetics of protein structures

Fig. 6 shows the evolution kinetics of the aforementioned spectral indicators, as well as that of ThT fluorescence intensity. As previously proposed,[20] four-stage kinetics occur in the amyloid fibrillation formation of HEWL with thermal/acid treatment: (a) exposure of the aromatic amino acid residues on side chains to the hydrophilic environment with partially unfolding of tertiary structures, (b) uncoiling of α-helical structures and aggregating to oligomers, (c) assembly of the oligomers into amyloidogenic filaments, and the formation of organized β-sheet structures in unbranched protofibrils, and (d) aggregation of the protofibrils to mature fibrils of cross β-sheet-rich structures.

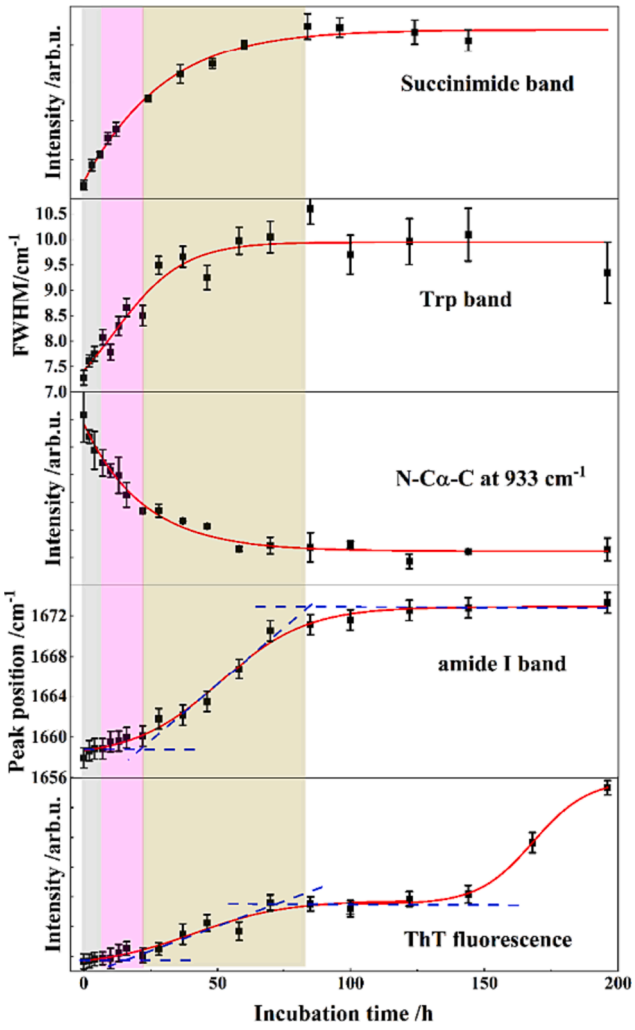


**Fig. 6.** Time-dependence curves of several Raman spectral indicators for succinimide intermediates, and protein secondary and tertiary structures, as well as the ThT fluorescence intensity.

As shown in Fig. 6, the two indicators of the succinimide intermediates (intensity at 1790 $cm^{-1}$) and the tertiary structures (Trp band) both exhibit single exponential growth processes. Both of them quickly increase during the initial stage, and reach 85 % of their own maxima at ~ 40 h and approach to saturation at ~ 85 h in current experimental conditions. Their almost identical kinetics strongly indicate a potential correlation between the destruction of tertiary structures and the formation of succinimide intermediates. We know that, along with partially unfolding, the protein tertiary structures are rapidly destroyed. As a result, aromatic amino-acid residue (such as Trp and Asp) side chains are exposed to the border region,[20] and meanwhile the neighboring Asp and Gly amino-acids on the protein backbone that are originally buried deep inside (such as Asp48 and Gly49, Asp66 and Gly67 of HEWL) are also exposed into the acidic aqueous environment. With the action of acid, the side chain –COOH of the L-Asp residue approaches the adjacent amide nitrogen of Gly, and then undergoes intermolecular cyclization to produce the succinimide intermediate as indicated in Scheme 1.

Notably, although the concentration of succinimide intermediates monotonously increases in the overall amyloid kinetics, their formation process does not appear to be related to changes in the secondary structure of proteins, as exhibited in Fig. 6. During the second stage (10–30 h, purple area in Fig. 6), α-helixes continue to uncoil almost to exhaustion as indicated by the Raman marker at 933 $cm^{-1}$, whereas no significant improvement is observed for the increasing rate of the percentage of succinimide intermediates. Likewise, no correlation is found for the formation of β-sheets and succinimide intermediates, as the blue shift of the amide I peak position and the enhancement of the ThT fluorescence intensity both do not show consistent trend with the variational rate of the succinimide concentration. These conclusions provide tangible evidences for our conjecture that the succinimide intermediates only play a significant role at the stage of oligomer formation throughout the overall amyloid formation process.

## 4. Conclusions

The succinimide intermediates are the nucleation points for amyloid fibril formation and can induce a non-native conformation in a fraction of soluble proteins to render amyloidogenicity and neurotoxicity.[7,8,13] Thus, *in situ* detection of succinimide intermediates during the amyloid fibrillation process in aqueous solutions is necessary for comprehensively evaluating the influence of posttranslational modifications on protein amyloidogenicity.[8] Here, we report a novel *in situ* Raman spectral fingerprint to trace the succinimide intermediates in aqueous solutions, that the peak at approximately 1790 $cm^{-1}$ arises from the imide carbonyl symmetric stretching of the formed succinimide ring. Whether derived from the Bz-Asp-Gly-$NH_2$ dipeptide or lysozyme, the fingerprint band is observed in solutions.

Furthermore, using this indicator we unravel the role of succinimide intermediates in the amyloid fibrillation formation of HEWL with thermal/acid treatment. It exhibits the identical kinetic behavior to the protein tertiary structures, and moreover, the similarity of the dipeptide and HEWL aggregation processes confirms that the succinimide intermediates play a crucial role at the stage of oligomer formation. These results provide more clues for the design of powerful, novel therapeutics for early events in neurodegenerative diseases.

## CRediT authorship contribution statement

**Ning Chen:** Data curation, Formal analysis, Investigation, Writing – original draft. **Yi Ren:** Data curation, Formal analysis, Investigation, Methodology. **Lei Xing:** Investigation, Methodology, Supervision, Validation. **Zhongqiang Liu:** Investigation, Methodology, Resources. **Lin Chen:** Validation, Visualization. **Shilin Liu:** Conceptualization, Funding acquisition, Project administration, Resources. **Xiaoguo Zhou:** Conceptualization, Project administration, Supervision, Writing – review & editing.

## Declaration of competing interest

The authors declare the following financial interests/personal relationships which may be considered as potential competing interests: Xiaoguo Zhou reports financial support was provided by National Natural Science Foundation of China.

## Data availability

Data will be made available on request.

## Acknowledgment

This work was supported by the National Natural Science Foundation of China (Grant Nos. 22073088 and 22027801). The quantum chemical calculations were performed on the supercomputing system in the Supercomputing Center of the University of Science and Technology of China.

## Appendix A. Supplementary data

Synthesis routes, HPLC, NMR and CID-MS/MS analyses of the

dipeptide, kinetic data processing for Raman indicators, and optimized geometries of the dipeptide and Asp/Gly monomers. Supplementary data to this article can be found online at https://doi.org/10.1016/j.saa.2024.123867.

## References


[1] A. Association, 2013 Alzheimer's disease facts and figures, Alzheimers Dement. 9 (2) (2013) 208–245.
[2] F. Chiti, C.M. Dobson, Protein misfolding, functional amyloid, and human disease, Annu. Rev. Biochem 75 (2006) 333–366.
[3] I.W. Hamley, Peptide fibrillization, Angew. Chem. Int. Ed. Engl. 46 (43) (2007) 8128–8147.
[4] T. Geiger, C.S. Deamidation, Isomerization, and racemization at asparaginyl and aspartyl residues in peptides. Succinimide-linked reactions that contribute to protein degradation, J. Biol. Chem. 262 (2) (1987) 785–794.
[5] M. Xie, D. Vander Velde, M. Morton, R.T. Borchardt, R.L. Schowen, pH-Induced Change in the Rate-Determining Step for the Hydrolysis of the Asp/Asn-Derived Cyclic-Imide Intermediate in Protein Degradation, J. Am. Chem. Soc. 118 (37) (1996) 8955–8956.
[6] S. Capasso, L. Mazzarella, F. Sica, A. Zagaria, S. Salvadorib, Spontaneous Cyclization of the Aspartic Acid Side Chain to the Succinimide Derivative, J. Chem. Soc., Chem. Commun (1992) 919–921.
[7] E.B. Dunkelberger, L.E. Buchanan, P. Marek, P. Cao, D.P. Raleigh, M.T. Zanni, Deamidation accelerates amyloid formation and alters amylin fiber structure, J. Am. Chem. Soc. 134 (30) (2012) 12658–12667.
[8] J. Orpiszewski, N. Schormann, B. Kluve-Beckerman, J.J. Liepnieks, M.D. Benson, Protein aging hypothesis of Alzheimer disease, FASEB J. 14 (9) (2000) 1255–1263.
[9] A.M. Pistorius, P.J. Groenen, W.J. de Grip, Infrared analysis of peptide succinimide derivatives, Int. J. Pept. Protein Res. 42 (6) (1993) 570–577.
[10] S. Noguchi, K. Miyawaki, Y. Satow, Succinimide and isoaspartate residues in the crystal structures of hen egg-white lysozyme complexed with tri-N-acetylchitotriose, J. Mol. Biol. 278 (1) (1998) 231–238.
[11] Y. Desfougères, J. Jardin, V. Lechevalier, S. Pezennec, F. Nau, Succinimidyl residue formation in hen egg-white lysozyme favors the formation of intermolecular covalent bonds without affecting its tertiary structure, Biomacromolecules 12 (1) (2011) 156–166.
[12] G. Muhammad, B. Saïd, C. Thomas, Structural consequences of dry heating on Beta-Lactoglobulin under controlled pH, Procedia Food Sci. 1 (2011) 391–398.
[13] S. Kumar, S. Prakash, K. Gupta, A. Dongre, P. Balaram, H. Balaram, Unexpected functional implication of a stable succinimide in the structural stability of Methanocaldococcus jannaschii glutaminase, Nat. Commun. 7 (2016) 12798.
[14] A. Zhang, P. Hu, P. MacGregor, Y. Xue, H. Fan, P. Suchecki, L. Olszewski, A. Liu, Understanding the conformational impact of chemical modifications on monoclonal antibodies with diverse sequence variation using hydrogen/deuterium exchange mass spectrometry and structural modeling, Anal. Chem. 86 (7) (2014) 3468–3475.
[15] D. Ouellette, C. Chumsae, A. Clabbers, C. Radziejewski, I. Correia, Comparison of the in vitro and in vivo stability of a succinimide intermediate observed on a therapeutic IgG1 molecule, MAbs 5 (3) (2013) 432–444.
[16] G.C. Chu, D. Chelius, G. Xiao, H.K. Khor, S. Coulibaly, P.V. Bondarenko, Accumulation of succinimide in a recombinant monoclonal antibody in mildly acidic buffers under elevated temperatures, Pharm. Res. 24 (6) (2007) 1145–1156.
[17] E. Frare, P. Polverino De Laureto, J. Zurdo, C.M. Dobson, A. Fontana, A highly amyloidogenic region of hen lysozyme, J. Mol. Biol. 340 (5) (2004) 1153–1165.
[18] J.C. Rochet, P.T. Lansbury, Amyloid fibrillogenesis: themes and variations, Curr. Opin. Struct. Biol. 10 (1) (2000) 60–68.
[19] R. Swaminathan, V.K. Ravi, S. Kumar, M.V.S. Kumar, N. Chandra, Lysozyme: a model protein for amyloid research, Adv. Protein Chem. Struct. Biol. 84 (2011) 63–111.
[20] L. Xing, W. Fan, N. Chen, M. Li, X. Zhou, S. Liu, Amyloid formation kinetics of hen egg white lysozyme under heat and acidic conditions revealed by Raman spectroscopy, J. Raman Spectrosc. 50 (5) (2019) 629–640.
[21] B. Ma, F. Zhang, X. Wang, X. Zhu, Investigating the inhibitory effects of zinc ions on amyloid fibril formation of hen egg-white lysozyme, Int. J. Biol. Macromol. 98 (2017) 717–722.
[22] L. Xing, N. Chen, W. Fan, M. Li, X. Zhou, S. Liu, Double-edged effects of aluminium ions on amyloid fibrillation of hen egg-white lysozyme, Int. J. Biol. Macromol. 132 (2019) 929–938.
[23] S. Bhattacharya, S. Ghosh, S. Dasgupta, A. Roy, Structural differences between native Hen egg white lysozyme and its fibrils under different environmental conditions, Spectrochim. Acta A Mol. Biomol. Spectrosc. 114 (2013) 368–376.
[24] S. Ghosh, N.K. Pandey, S. Bhattacharya, A. Roy, S. Dasgupta, Fibrillation of hen egg white lysozyme triggers reduction of copper(II), Int. J. Biol. Macromol. 51 (1–2) (2012) 1–6.
[25] S. Ghosh, N.K. Pandey, S. Bhattacharya, A. Roy, N.V. Nagy, S. Dasgupta, Evidence of two oxidation states of copper during aggregation of hen egg white lysozyme (HEWL), Int. J. Biol. Macromol. 76 (2015) 1–9.
[26] A.B. Bowman, G.F. Kwakye, E. Herrero Hernández, M. Aschner, Role of manganese in neurodegenerative diseases, J. Trace Elem. Med Biol. 25 (4) (2011) 191–203.
[27] G.F. Kwakye, M.M.B. Paoliello, S. Mukhopadhyay, A.B. Bowman, M. Aschner, Manganese-Induced Parkinsonism and Parkinson's Disease: Shared and Distinguishable Features, Int. J. Environ. Res. Public Health 12 (7) (2015) 7519–7540.
[28] N. Nishimura, The mechanism of cadmium-induced lysozyme enhancement in rabbit kidney, Arch. Toxicol. 61 (1987) 105–115.
[29] L.-F. Jiang, T.-M. Yao, Z.-L. Zhu, C. Wang, L.-N. Ji, Impacts of Cd(II) on the conformation and self-aggregation of Alzheimer's tau fragment corresponding to the third repeat of microtubule-binding domain, Biochim. Biophys. Acta 1774 (11) (2007) 1414–1421.
[30] J. Wang, X. Yang, J. Wang, C. Xu, W. Zhang, R. Liu, W. Zong, Probing the binding interaction between cadmium(ii) chloride and lysozyme, New J. Chem. 40 (4) (2016) 3738–3746.
[31] S. Ghasemzadeh, G.H. Riazi, Inhibition of Tau amyloid fibril formation by folic acid: In-vitro and theoretical studies, Int. J. Biol. Macromol. 154 (2020) 1505–1516.
[32] L. Jin, W. Gao, C. Liu, N. Zhang, S. Mukherjee, R. Zhang, H. Dong, A. Bhunia, Z. Bednarikova, Z. Gazova, M. Liu, J. Han, H.-C. Siebert, Investigating the inhibitory effects of entacapone on amyloid fibril formation of human lysozyme, Int. J. Biol. Macromol. 161 (2020) 1393–1404.
[33] W. Fan, X. Chen, L. Liu, N. Chen, X. Zhou, Z. Zhang, S. Liu, Concentration-dependent influence of silver nanoparticles on amyloid fibrillation kinetics of hen egg-white lysozyme, Chin. J. Chem. Phys. 34 (4) (2021) 393–405.
[34] W. Fan, L. Xing, N. Chen, X. Zhou, Y. Yu, S. Liu, Promotion Effect of Succinimide on Amyloid Fibrillation of Hen Egg-White Lysozyme, J. Phys. Chem. B 123 (38) (2019) 8057–8064.
[35] P.G. Kabadi, P.K. Sankaran, D.V. Palanivelu, L. Adhikary, A. Khedkar, A. Chatterjee, Mass Spectrometry Based Mechanistic Insights into Formation of Tris Conjugates: Implications on Protein Biopharmaceutics, J. Am. Soc. Mass Spectrom. 27 (10) (2016) 1677–1685.
[36] M. Simonovic, K. Volz, Atomic resolution structure of a succinimide intermediate in E. coli CheY, J. Mol. Biol. 322 (4) (2002) 663–667.
[37] R.C. Stephenson, S. Clarke, Succinimide formation from aspartyl and asparaginyl peptides as a model for the spontaneous degradation of proteins, J. Biol. Chem. 264 (11) (1989) 6164–6170.
[38] V. Shashilov, M. Xu, V.V. Ermolenkov, L. Fredriksen, I.K. Lednev, Probing a fibrillation nucleus directly by deep ultraviolet Raman spectroscopy, J. Am. Chem. Soc. 129 (22) (2007) 6972–6973.
[39] V.A. Shashilov, I.K. Lednev, 2D correlation deep UV resonance raman spectroscopy of early events of lysozyme fibrillation: kinetic mechanism and potential interpretation pitfalls, J. Am. Chem. Soc. 130 (1) (2008) 309–317.
[40] S.-Y. Ow, D.E. Dunstan, The effect of concentration, temperature and stirring on hen egg white lysozyme amyloid formation, Soft Matter 9 (40) (2013) 9692–9701.
[41] L. Chen, W. Zhu, K. Lin, N. Hu, Y. Yu, X. Zhou, L.-F. Yuan, S.-M. Hu, Y. Luo, Identification of alcohol conformers by Raman spectra in the C-H stretching region, Chem. A Eur. J. 119 (13) (2015) 3209–3217.
[42] L. Xing, K. Lin, X. Zhou, S. Liu, Y. Luo, Multistate Mechanism of Lysozyme Denaturation through Synchronous Analysis of Raman Spectra, J. Phys. Chem. B 120 (41) (2016) 10660–10667.
[43] K. Lin, X. Zhou, Y. Luo, S. Liu, The microscopic structure of liquid methanol from Raman spectroscopy, J. Phys. Chem. B 114 (10) (2010) 3567–3573.
[44] Y. Wang, W. Zhu, K. Lin, L. Yuan, X. Zhou, S. Liu, Ratiometric detection of Raman hydration shell spectra, J. Raman Spectrosc. 47 (10) (2016) 1231–1238.
[45] M. Frisch, G.W. Trucks, H.B. Schlegel, G.E. Scuseria, M.A. Robb, J.R. Cheeseman, G. Scalmani, V. Barone, B. Mennucci, G. Petersson, Gaussian 09, revision a. 02, gaussian. Gaussian 09, revision a. 02, gaussian 2009, 200.
[46] I.M. Alecu, J. Zheng, Y. Zhao, D.G. Truhlar, Computational Thermochemistry: Scale Factor Databases and Scale Factors for Vibrational Frequencies Obtained from Electronic Model Chemistries, J. Chem. Theory Comput. 6 (9) (2010) 2872–2887.
[47] R. Horvath, K.C. Gordon, Understanding excited-state structure in metal polypyridyl complexes using resonance Raman excitation profiles, time-resolved resonance Raman spectroscopy and density functional theory, Coord. Chem. Rev. 254 (21–22) (2010) 2505–2518.
[48] S.A. Oladepo, K. Xiong, Z. Hong, S.A. Asher, J. Handen, I.K. Lednev, UV resonance Raman investigations of peptide and protein structure and dynamics, Chem. Rev. 112 (5) (2012) 2604–2628.
[49] S. Stewart, P.M. Fredericks, Surface-enhanced Raman spectroscopy of peptides and proteins adsorbed on an electrochemically prepared silver surface, Spectrochim. Acta A Mol. Biomol. Spectrosc. 55 (7) (1999) 1615–1640.
[50] T. Nakabayashi, K. Kosugi, N. Nishi, Liquid structure of acetic acid studied by Raman spectroscopy and ab initio molecular orbital calculations, Chem. A Eur. J. 103 (43) (1999) 8595–8603.
[51] D. Kurouski, R.P. van Duyne, I.K. Lednev, Exploring the structure and formation mechanism of amyloid fibrils by Raman spectroscopy: a review, Analyst 140 (15) (2015) 4967–4980.
[52] D.M. Carey, G.M. Korenowski, Measurement of the Raman spectrum of liquid water, J. Chem. Phys. 108 (7) (1998) 2669–2675.
[53] G.E. Walrafen, L.a. Blatz, Weak Raman bands from water, J. Chem. Phys. 59 (5) (1973) 2646–2650.
[54] Y. Zou, W. Hao, H. Li, Y. Gao, Y. Sun, G. Ma, New insight into amyloid fibril formation of hen egg white lysozyme using a two-step temperature-dependent FTIR approach, J. Phys. Chem. B 118 (33) (2014) 9834–9843.
[55] S.E. Hill, J. Robinson, G. Matthews, M. Muschol, Amyloid protofibrils of lysozyme nucleate and grow via oligomer fusion, Biophys. J. 96 (9) (2009) 3781–3790.
[56] L.N. Arnaudov, R. de Vries, Thermally induced fibrillar aggregation of hen egg white lysozyme, Biophys. J. 88 (1) (2005) 515–526.
[57] S. Dolui, A. Roy, U. Pal, A. Saha, N.C. Maiti, Structural Insight of Amyloidogenic Intermediates of Human Insulin, ACS Omega 3 (2) (2018) 2452–2462.

[58] A. Barth, C. Zscherp, What vibrations tell us about proteins, Q. Rev. Biophys. 35 (4) (2002) 369–430.
[59] K. Huang, N.C. Maiti, N.B. Phillips, P.R. Carey, M.A. Weiss, Structure-specific effects of protein topology on cross-beta assembly: studies of insulin fibrillation, Biochemistry 45 (34) (2006) 10278–10293.
[60] S. Mangialardo, F. Piccirilli, A. Perucchi, P. Dore, P. Postorino, Raman analysis of insulin denaturation induced by high-pressure and thermal treatments, J. Raman Spectrosc. 43 (6) (2012) 692–700.